Comparisons of computational fluid dynamics solutions of static and manoeuvring fighter aircraft with flight test data

D R McDaniel[1,2*], **R M Cummings**[1], **K Bergeron**[1], **S A Morton**[3], and **J P Dean**[3]
[1]Department of Aeronautics, US Air Force Academy, Colorado, USA
[2]Now at: University of Alabama at Birmingham, Alabama, USA
[3]US Air Force SEEK EAGLE Office, Eglin AFB, Florida, USA

The manuscript was received on 7 July 2008 and was accepted after revision for publication on 7 October 2008.

DOI: 10.1243/09544100JAERO411

Abstract: As the capabilities of computational fluid dynamics (CFD) to model full aircraft configurations improve, and the speeds of massively parallel machines increase, it is expected that CFD simulations will be used more and more to steer or in some cases even replace traditional flight test analyses. The mission of the US Air Force SEEK EAGLE office is to clear any new weapon configurations and loadings for operational use. As more complex weapons are developed and highly asymmetric loadings are requested, the SEEK EAGLE office is tasked with providing operational clearances for literally thousands of different flight configurations. High-fidelity CFD simulations employing the turbulent Navier–Stokes equations are in a prime position to help reduce some of the required wind-tunnel and/or flight test workload. However, these types of CFD simulations are still too time consuming to populate a full stability and control parameter database in a brute-force manner. This article reviews results previously published by the authors, which validate the ability of high-fidelity CFD techniques to compute static force and moment characteristics of aircraft configurations. A methodology to generate efficient but non-linear reduced-order aerodynamic loads models from dynamic CFD solutions, which in-turn may be used to quickly analyse various stability and control characteristics at a particular flight condition, is introduced, and the results based on the US Air Force F-16C fighter aircraft that exemplify the process are discussed.

Keywords: computational fluid dynamics, stability and control, reduced-order model, flight test, System Identification Programs for Aircraft

1 INTRODUCTION

The determination of the stability and control characteristics of a new fighter aircraft design is an iterative process encompassing computational, wind-tunnel, and flight test modelling techniques. This is especially true when considering operation in areas of the flight envelope where aerodynamic effects due to things such as aeroelastic surface motion or high angle of attack flight are important. Commonly used aerodynamic modelling tools are efficient but predominantly linear and therefore do not adequately capture some non-linear aerodynamic effects such as vortex-boundary layer, shock–shock, and shock–vortex-boundary layer interactions. These non-linear effects can lead to aircraft instabilities such as abrupt wing stall, vortex ring state, tail buffet, and limit cycle oscillations, which can either limit the aircraft life span or operational envelope.

Practically, every fighter program since 1960 has had some of these costly non-linear aerodynamic or fluid–structure interaction issues discovered in the flight test. In an article by a Boeing Technical Fellow, Dr Rudy Yurkovich [**1**], a review of the Boeing F-15, F/A-18A and AV-8B programs were described from an aeroelasticity perspective. In the F-15 program, the empennage exhibited flutter issues and considerable aeroelastic wind-tunnel and flight testing was required to repair the surfaces and to ensure the required speed margins that exist in the operational envelope. In the F/A-18A program, the combination of

*Corresponding author: University of Alabama at Birmingham, Alabama, USA.
email: drmcd@uab.edu; david.mcdaniel.ctr@eglin.af.mil

a thin wing and leading-edge flaps created difficulty in predicting divergence-driven flutter mechanism for high-speed conditions. In the AV-8B program, a thick super-critical airfoil resulted in a deep transonic flutter speed dip, not predicted in advance. Fortunately, the thick wing section allowed for torsional stiffness that compensated for the reduction in flutter speed in the transonic Mach range. In other publications, tail buffet of the F/A-18C at high angles of attack was described where leading-edge extension vortex breakdown created unsteady tail loads and early tail fatigue not predicted in simulation [**2**]. Northrup–Grumman designers described a residual pitch oscillation of the B-2 Bomber not predicted by simulation before the flight test, which required extensive flight control re-design [**3**]. In each of these aircraft programs, these non-linear aerodynamic issues were solved and all of these aircrafts have proven themselves to be exceptional. However, one has to wonder how many additional aircrafts could have been purchased if a truly predictive method had existed for the entire operational envelope that would have identified these issues before the first item was manufactured. These issues will only become more pronounced with future fighter aircraft designs[**4**]. This is especially true for unmanned combat air vehicles where man-rating requirements are no longer a factor when determining manoeuvring limits.

Similar instabilities can also surface on proven and fielded fighter aircraft at seemingly uneventful flight conditions when considering the advanced weaponry now available and the complex asymmetric aircraft loadings that the warfighters are currently requesting as a result. The US Air Force SEEK EAGLE office (AFSEO) is tasked with providing operational flight clearances for weapons loadings on all US Air Force aircrafts. There have been instances where particular weapons' configurations have led to some of the instabilities discussed previously even at nominal cruise conditions. These instabilities normally lead to a restriction on the allowable weapons loadings and/or the employment envelope. On the other hand, the authors have previously discussed case studies of flight test programs at AFSEO where many resources were expended only to discover that the stability and control characteristics and handling qualities of the new store configurations under study were very benign [**5**]. Although these uneventful results are desirable and beneficial to the warfighter, they are not optimal in terms of resource allocation. Additionally, these are common occurrences when one reviews the extensive store compatibility flight test history of the F-16 fighter aircraft.

Three traditional methods exist to determine the stability and control characteristics. The first, and the most accurate method, involves flight testing the actual aircraft [**6**–**8**]. Unfortunately, these tests are very expensive, time consuming, and require an operational aircraft, which may not be readily available. Additionally, there are safety issues that are normally mitigated by a thorough review board and approval process. It can take anywhere from many months to a few years to complete a flight test program depending on the number and type of required tests. The second method is to use wind-tunnel testing of scale models [**9**]. This is also a time-consuming and expensive process. Additionally, there are blockage, scaling, and Reynolds-number effects together with support interference issues that prevent the proper modelling of the full-scale vehicle behaviour. Also, changes to the actual aircraft geometry may invalidate wind-tunnel test data. The final method employs a combination of data sheets, linear aerodynamic theory, and empirical relations [**10**, **11**]. This method has met with great success due to its simplicity, but its accuracy is limited – although the basic lift and drag characteristics of high-performance aircrafts such as the F-16 and F-18 may be predicted fairly well at benign flight conditions, it is very difficult if not impossible to accurately capture the unsteady and dynamic aerodynamic effects of manoeuvring the fighter aircraft with these techniques.

Clearly, high-fidelity computational tools capable of accurately predicting troublesome stability and control characteristics would be a welcome addition to existing analysis techniques. Such tools would help reduce total development costs of new fighter aircrafts and maximize weapons employment envelopes of existing fighter aircrafts. Accurate and efficient predictive tools capable of identifying configurations susceptible to handling quality instabilities prior to the flight test are critical to optimizing flight test funds, minimizing risk to aircrews, and delivering maximum capability to the warfighter.

This article focuses on the use of high-fidelity computational fluid dynamics (CFD) to compute force and moment characteristics of static and dynamic (manoeuvring) fighter aircrafts. A methodology to generate efficient, yet non-linear reduced-order aerodynamic loads models from dynamic CFD solutions, which in-turn may be used to quickly analyse various stability (and eventually control) characteristics at a particular flight condition, is also introduced. First, some current approaches to stability and control analysis are reviewed. Next, the reduced-order aerodynamic loads modelling approach is discussed. Then, previous full-aircraft computations and associated flight test comparisons by the authors are reviewed, which speak to the level of fidelity achievable with modern flow solvers. Finally, the reduced-order non-linear modelling approach is demonstrated through some initial results and comparisons with an aerodynamic database derived from the test data.

2 BACKGROUND

Computational techniques have been used since the mid-1960s [**4**] to augment proven wind-tunnel and flight test techniques to determine stability and control characteristics of the aircraft. As discussed previously, only turbulent Navier–Stokes CFD solvers are capable of capturing the aerodynamic phenomena that lead to various static and dynamic instabilities. These solvers have reached a level of robustness and maturity to support routine, everyday use on relatively inexpensive computer clusters. In addition, CFD can increase our understanding of the causes and types of separated flows affecting stability and control (S&C) prediction. CFD has its own limitations, of course, such as turbulence and transition modelling, to name a few. However, the large body of previous work [**12–18**] performed by researchers at the US Air Force Academy using the unstructured mesh solver *Cobalt* [**19**] coupled with a detached-eddy simulation (DES) turbulence treatment, adaptive mesh refinement, six degree of freedom (6 DOF) motion, and deforming grids for aero-elasticity has led to a high-fidelity capability for computing stability and control characteristics.

Given a valid computational technique that is capable of adequately computing full-aircraft force and moment coefficients (and subsequently the desired force and moment derivatives), there are a number of avenues one could follow to generate the needed aerodynamic 'database' for the problem at hand. For new vehicle designs, researchers at NASA Ames have attempted to perform a 'brute-force' approach to filling a stability and control database [**20**, **21**]. They found that a reasonable database for static stability and control derivatives would include on the order of '30 different angles of attack, 20 different Mach numbers, and 5 different side-slip angles, each for a number of different geometry configurations or control surface deflections' [**21**]. This equates to an estimated 30 000 CFD solutions if ten configuration/control surface deflections are analysed. They demonstrated a simulation approach on a large parallel machine with good success but the simulations were limited primarily to the Euler equations and fairly coarse grids. To perform simulations necessary to capture the nonlinear phenomena discussed above, grids on the order of 5–10 million cells would be necessary for half-span and 10–20 million cells for full-span geometries using the Navier–Stokes equations with a relevant turbulence treatment. The wall clock time to compute these solutions on a 256-processor IBM P4+ for a 16-million cell grid is 1.4 million h or 158 years. Other than the obvious resource limitations, there are two major problems with this approach. First, the above approach does not account for dynamic derivatives necessary for an all-encompassing vehicle design, and second, the method assumes that the discrete set of points computed captures all of the relevant nonlinearities in the stability derivatives when clearly a 'bump in the curve' could exist between the chosen test points. Other approaches investigated by NASA Ames researchers to make the process more computationally tractable while overcoming these limitations have been to combine many low-order solutions with a few high-order solutions [**22**, **23**], the automation of a Cartesian CFD method by leveraging existing stand-alone applications to perform isolated steady-state simulations and gluing them together with control scripts [**24**], and reduced-frequency modelling [**25**].

With regard to the stability analysis of the existing aircraft with configuration changes (e.g. new weapon loadings), a number of flight conditions are analysed/cleared by 'analogy'. In other words, if the flight condition and outer mold line of the new vehicle configuration are analogous to a previously tested configuration, then the desired test point may be assumed to be acceptable without ever computing any stability data. This method has become all but a requirement at AFSEO due to the increasing number of new configurations that must be cleared each year. Figure 1, consolidated from [**26**] with permission, shows that ~1–2 per cent of the total number of vehicle configurations that need to be analysed for fluid–structure instabilities to support a new store compatibility clearance are actually flight tested. Also, while this might have resulted in <10 flight test configurations 10 years ago, on the order of 75 different flight test configurations are required today. It can be assumed that a corresponding number of configurations must be analysed for S&C/handling qualities issues.

While high-fidelity CFD techniques (even those including aeroelastic effects) should never fully replace flight testing the actual vehicle, it is possible that the 1–2 per cent of the required flight test configurations that need to be cleared by new results could be reduced even further by these computational methods.

A final computational technique to determine aircraft stability characteristics has emerged only within the last few years due to the increasing availability of massively parallel machines. While the computation of static stability derivatives can be done with most off-the-shelf CFD tools, the prediction of dynamic derivatives requires a time-dependent prescribed motion capability in the flow solver as well as prescribed motions ('manoeuvres') that adequately excite the desired aerodynamics by generating changes in the angle of attack, angle of sideslip, and body axis rotation rates. An excellent example of this application is given in [**27**]. Such high-fidelity CFD offers several unique capabilities that complement experimental testing techniques for obtaining these aerodynamic parameters, but without their limitations. The physical limitations and kinematic restrictions of wind tunnel

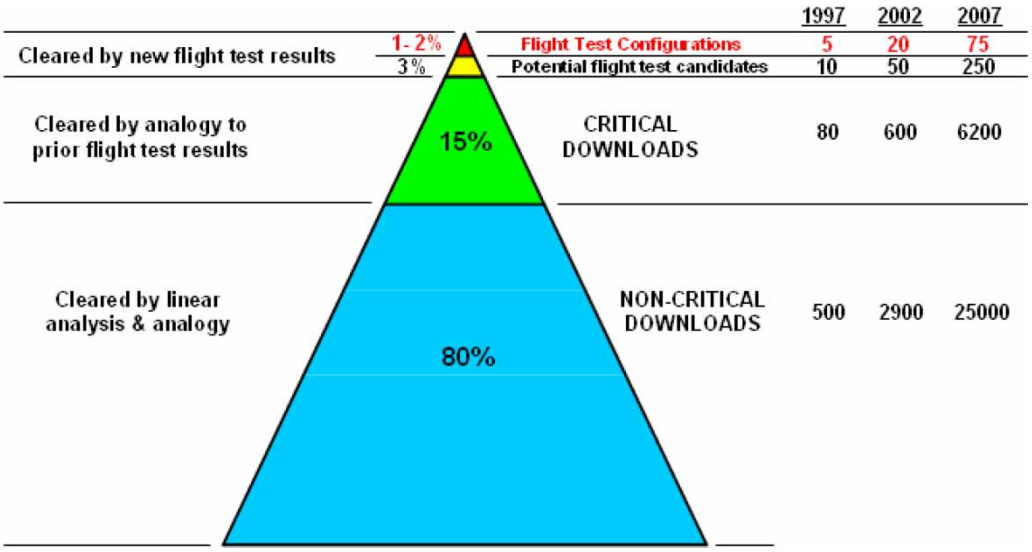

Fig. 1 Relative number of critical flight test configurations to support store compatibility clearances at AFSEO (adapted from reference [**26**] with permission)

testing including model motion as well as the interference effects of the model support are not factors in the computational analysis. Flight tests are limited by the fact that only 'flyable' manoeuvres are possible where many of the parameters in common aerodynamic models are lumped together with no way to determine the independent effects. With CFD, it is possible to prescribe any type of aircraft motion in a flowfield to determine damping and cross-derivatives individually since arbitrary dynamic manoeuvers are possible. For example, a pitch oscillation can be combined with a manoeuvre where no pitch rate exists (continuous or pulsed plunge) to remove the effect of $\dot{\alpha}$ on the combined derivative $\bar{C}_{L_q} = C_{L_q} + C_{L_{\dot{\alpha}}}$. This is the technique on which the reduced-order non-linear loads models discussed in this article are based.

3 MODELLING APPROACH

The aircraft stability analysis approach proposed here does not confront the problem from the same point of view as discussed previously. Instead, a small number of prescribed motions are implemented, and non-linear loads models are identified from the resulting time-accurate dynamic solution. Figure 2 depicts

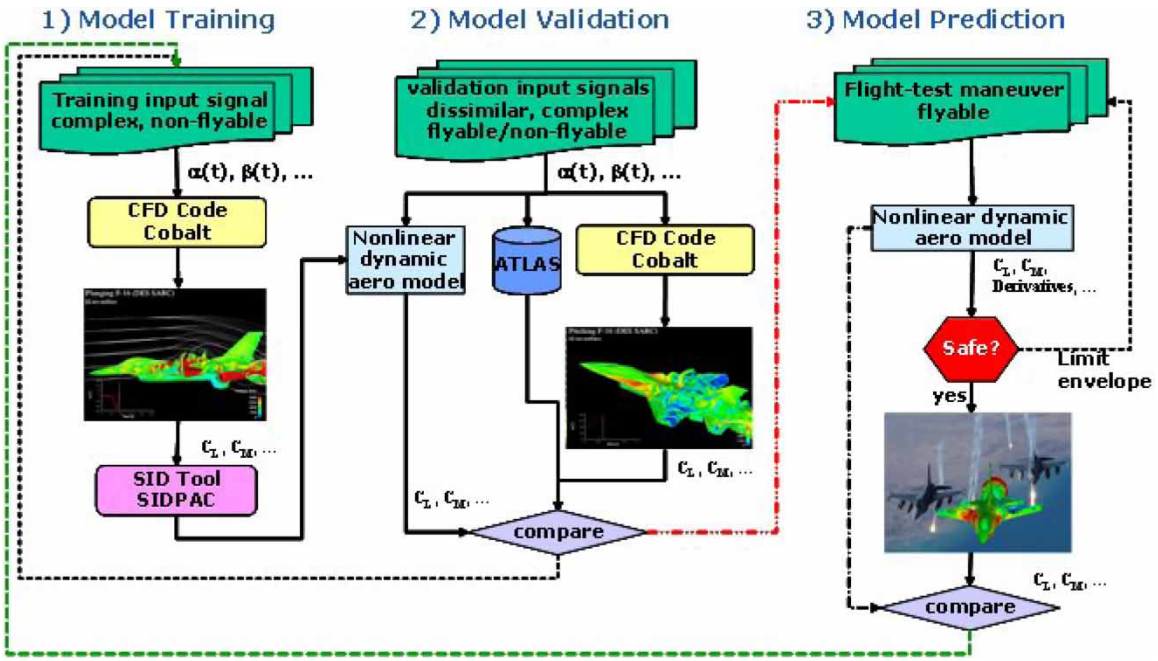

Fig. 2 Stability and control model build process

this process graphically. The first step in the method is to build a geometric representation of the complete aircraft of interest (including stores, control surfaces, inner loop control laws, aeroelastic effects, and so on.). Next, simulations are performed of manoeuvres designed to excite the relevant flow physics that will be encountered during actual missions in all three axes, roll, pitch, and yaw. These simulations are termed 'computational manoeuvres', since they may be unreasonable to fly due to actual aircraft or pilot limits. Next, a mathematical model is built of the aircraft response using system identification (SID). Then, the model is tested by comparing CFD simulations against model predictions of simulations expected to be encountered in flight. Finally, predictions of all flight test points are made using the model before flight tests are conducted to determine the expected behaviour of the actual aircraft. The following sub-sections describe the individual elements of the flow solver and SID method necessary for the process.

3.1 Flow solver

Computations are performed using the commercial flow solver *Cobalt*. *Cobalt* is a cell-centered, finite-volume CFD code. It solves the unsteady, three-dimensional, compressible Reynolds-averaged Navier–Stokes (RANS) equations on hybrid unstructured grids. Its foundation is based on Godunov's first-order accurate, exact Riemann solver. Second-order spatial accuracy is obtained through a least-squares reconstruction. A Newton sub-iteration method is used in the solution of the system of equations to improve time accuracy of the point-implicit method. Strang *et al.* [**19**] validated the numerical method on a number of problems, including the Spalart–Allmaras (SA) model, which forms the core for the DES model available in *Cobalt*. Tomaro *et al.* [**28**] converted the code from explicit to implicit, enabling CFL numbers as high as 10^6. Grismer *et al.* [**29**] parallelized the code, yielding linear speed up on as many as 2800 processors. The parallel METIS (PARMETIS) domain decomposition library of Karypis *et al.* [**30**] is also incorporated into *Cobalt*. New capabilities include rigid-body and 6 DOF motion, equilibrium air physics, and delayed DES [**31**] and overset grids in release *Cobalt V4.0*. A coupled aeroelastic simulation capability is also being developed.

3.2 Chirp grid motion inputs

One of the important elements of any SID process is the definition of an input signal that sufficiently excites the dynamics of the system under study (in this particular case, the aerodynamic system). Based on a cursory evaluation of a number of different motion types [**32**], it was determined that a simple chirp input applied to either a plunge or a rotational grid motion led to reduced-order models with the best overall dynamic predictive capability. This is most likely due to the fact that the broad range of frequencies in the chirp signal excites the aerodynamic system over a large range of angle of attack, angle of sideslip, pitch rate, and so on. The relationship used to create these chirp signals is the same as that used in the 'chirp' function in MATLAB® and is given in equation 1

$$s(t) = \cos\left[2\pi\left(\frac{\beta}{\lambda+1}t^{\lambda+1} + f_1 t + \frac{\phi}{360}\right)\right] \tag{1}$$

where

$$\beta = \left(\frac{f_2 - f_1}{t_2^{\lambda}}\right)$$

The parameters f_1 and f_2 denote the low and high limits of the chirp frequency bandwidth, respectively. The parameter t_2 is the time length of the chirp signal, and the parameter ϕ provides the ability to apply a phase shift to the signal as needed to help control whether or not the signal is biased relative to the starting amplitude. For a given signal length and bandwidth, the parameter λ controls the rate at which the signal traverses the requested frequency range. A value of $\lambda = 1.0$ corresponds to a linear change in frequency, whereas a value of $\lambda = 2.0$ corresponds to a quadratic change in frequency, and so forth. Figure 3 shows the variation of frequency with time for a number of different values of this parameter.

Figure 4 shows pitch axis rotational input signals for two different values of λ. The authors are currently investigating the effect of different values of the λ parameter on the ability of models resulting from the various pitch chirp manoeuvres to predict both static and dynamic validation data. Past experience has shown that a linear change in frequency in the chirp signal tends to result in poor model predictions of static data. Chirp signals with higher λ values, which effectively dwell at the lower frequencies, as seen in Fig. 4, will hopefully improve these static predictions.

3.3 SID analysis

SID is the process of constructing a mathematical model from input and output data for a system under testing, and characterizing the system uncertainties and measurement noises [**33**]. The mathematical model structure can take various forms depending on the intended use. SID has traditionally been applied to wind-tunnel and flight test data to obtain accurate and comprehensive mathematical models of aircraft aerodynamics for aircraft flight simulation, control system design and evaluation, and dynamic analysis. A very comprehensive review of SID applied to aircraft can be found in Morelli and Klein [**34**, **35**] and Jategaonkar *et al.* [**36**, **37**].

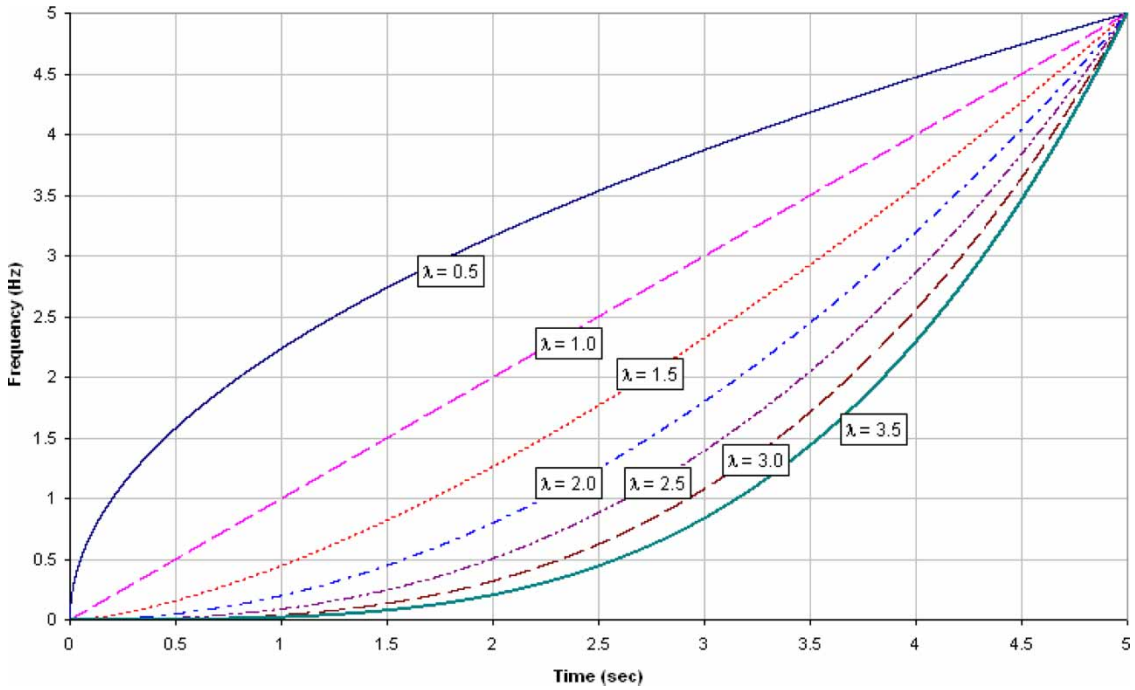

Fig. 3 Frequency variation with time for various values of the chirp λ parameter

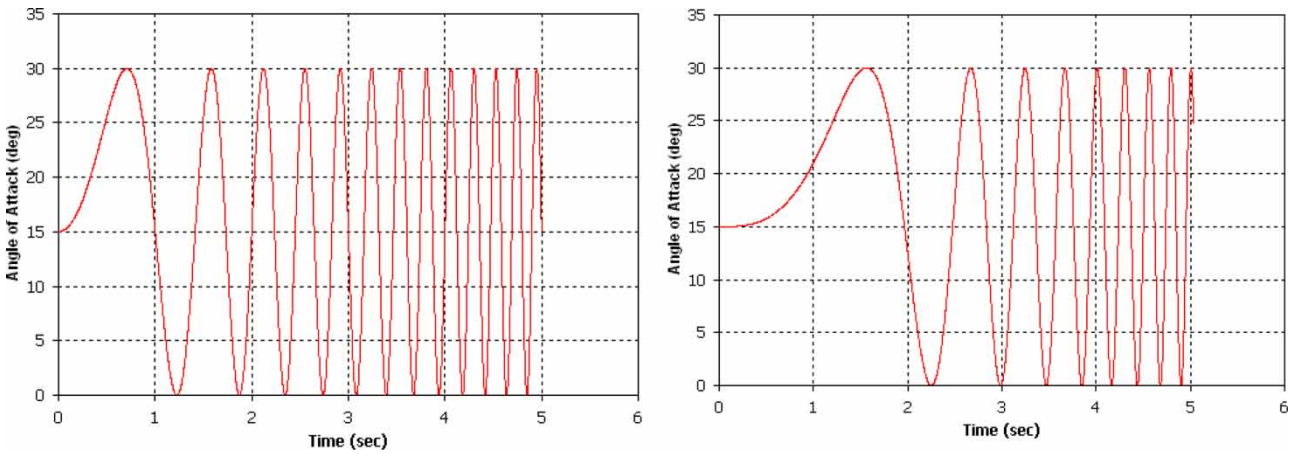

Fig. 4 Angle of attack histories for pitch-axis chirp motions with attack histories for $\lambda = 1.0$ (left) and $\lambda = 2.0$ (right)

Aircraft SID can be used in cooperation with CFD to take advantage of the strengths, both of SID and CFD or having one approach fill in the gaps where the other cannot be used effectively [**34**]. The wide range of SID tools that have been developed for aircraft SID can easily be used to analyse CFD data computed for aircraft in prescribed motion. Here, we follow the global non-linear parameter modelling technique proposed by Morelli [**38**] to describe the functional dependence between the motion and the computed aerodynamic response in terms of force and moment coefficients. The goal is to find a model that has adequate complexity to capture the non-linearities while keeping the number of terms in the model low. The latter requirement improves the ability to identify model parameters, resulting in a more accurate model with good predictive capabilities. The modelling effort is global because the independent variables ($\alpha, \dot{\alpha}, \beta$, etc.) are varied over a large range. Globally, valid analytical models and their associated smooth gradients are useful for optimization, robust non-linear control design, and global non-linear stability and control analysis. For example, a particular model may be differentiated directly to compute any desired stability or control derivative.

A range of SID techniques are implemented in a collection of computer programs called System IDentification Programs for AirCraft (SIDPAC) [**39**]. SIDPAC was developed at NASA Langley Research Center for analysing and modelling flight-test and wind-tunnel

data. SIDPAC addresses a wide range of SID problems in a common MATLAB environment. It includes routines for experiment design, data conditioning, data compatibility analysis, model structure determination, equation-error and output-error parameter estimation in both the time and frequency domains, real-time and recursive parameter estimation, low-order equivalent SID, estimated parameter error calculation, linear and non-linear simulation, plotting, and three-dimensional visualization. These tools are used for the current research.

3.4 Examples

Three different examples are provided in this section. The first two examples are comprised of static CFD calculations of full fighter aircraft configurations and associated comparisons with available flight-test data. These examples demonstrate the capabilities of high-fidelity CFD to accurately compute full-aircraft flowfields and corresponding forces and moments. The last example is taken from an ongoing multi-year project where dynamic CFD calculations with prescribed motion are being used in concert with the modelling capability described above. In this example, comparisons are made with an available stability and control database derived from wind-tunnel and flight-test data.

3.4.1 F-16XL

The Cranked-Arrow Wing Aerodynamics Project (CAWAP) provided the CFD community with an excellent database for complex aerodynamic validation and evaluation purposes [**40**, **41**]. The project focused on the understanding of the flow phenomena encountered on a cranked-arrow wing relevant to advanced fighter and transport aircraft. The subject of investigation was the F-16XL aircraft, as shown in Fig. 5. The Cranked-Arrow Wing Aerodynamics Project International (CAWAPI), which was initiated by NASA as a follow-on project to the CAWAP, allowed for a larger international community of researchers to participate in predicting the aerodynamics of the F-16XL. Along with the Vortex Flow Experiment 2 [**42**], CAWAPI was incorporated under the NATO RTO Task Group AVT-113. The objective of the CAWAPI facet was to allow a comprehensive validation and evaluation of CFD methods against the CAWAP flight database [**40**, **41**]. A number of researchers simulated the flowfield of the F-16XL at a variety of flight test conditions using different numerical approaches, including structured, block, and unstructured grids, as well as various turbulence models and numerical algorithms. This type of full-scale aircraft configuration provides many challenges to state-of-the-art CFD flow prediction, including the ability to accurately predict unsteady flowfields at flight Reynolds numbers.

Fig. 5 F-16XL aircraft (© NASA Dryden Flight Research Center)

The specific aim of the this work is to perform time-accurate calculations for flow over the F-16XL at full-scale flight Reynolds numbers, and to document the effects of applying DES at conditions consistent with the complex flow phenomenon. Understanding the unsteady flowfield can lead to improved knowledge about the flight characteristics of the aircraft that can be overlooked by steady RANS or unsteady RANS (URANS) calculations. Although unsteady CFD predictions of full-scale aircraft are relatively expensive to perform, their values have been shown to be important in many of the studies referenced above. Abrupt wing stall [**13**], for example, could not have been predicted using a URANS CFD approach and the aerodynamics of manoeuvring aircraft cannot be adequately predicted without the use of a hybrid RANS/large-eddy simulation (LES) approach. Results show that there are several flow features of F-16XL that are predicted correctly using an unsteady approach. Details about the computations may be found in reference [**43**].

There were seven CAWAP flight conditions chosen by the CAWAPI RTO Task Group as candidates for comparison. Of the seven cases, five of them were assumed to be symmetric conditions. Only half-span grids were used in these computations, although there is up to a $+0.725$ and -0.133° sideslip error in the assumption (see reference [**43**] for details). Flight condition 7 (FC7 in Table 1) is a medium angle-of-attack condition at subsonic Mach number and low altitudes. The Reynolds number (based on mean aerodynamic chord) is 44.4 million for flight condition 7, which offers challenges in grid resolution, especially within the boundary layer where the normal spacing of the

Table 1 FC7 flight condition definition

Mach	Altitude (ft)	AOA (°)	Beta actual (°)	Beta comp (°)	Re_{mac}
0.304	5000	11.89	−0.133	0	4.44E+07

grid points above the surface in the viscous region is still within an average $y+$ of one.

Because the numerical results for these cases were at least partially unsteady (due to the interaction of the leading-edge vortex with the air dam over the wing), solutions were run using a hybrid RANS/LES model, specifically the SA turbulence model with rotation corrections (SARC) in conjunction with DES (notated as SARCDES in the following results). DES requires the use of small time steps to accurately resolve the time scales of the large eddies within the flow, and therefore, a time-accurate method is required to obtain the results. These unsteady results vary in time and are difficult to compare with flight-test data; hence, the time-accurate unsteady solutions are averaged in time over 2000 iterations, and the minimum and maximum instantaneous values observed during these time span are noted. Figure 6 shows both the instantaneous and time-averaged predictions of the off-surface vortical structures (Fig. 6(a)) and the surface pressure distribution (Fig. 6(b)) for flight condition 7. It is apparent that the dominant features of the flowfield are the leading-edge vortex, the air dam vortex, the outer wing vortex, and a complicated set of vortices from the AIM-9 fins and fore body. It can also be seen that the leading-edge vortex changes characteristic from a coherent structure to a complex structure with helical windings, similar to vortex breakdown, in the region of the actuator pod. It is also interesting to note that the helical vortex structure is above the vortex emanating from the air dam creating a very complex structure. Notice that while time-averaged vortices (both the leading-edge and outer wing vortices) appear, a great deal of flow resolution is lost in the averaging process. In spite of this, however, the surface pressures differ only slightly between the two results.

Figure 7 depicts the flight-test surface pressure coefficient, Cp, data compared to the computed time-averaged Cp, computed minimum and maximum Cp at a given location, and the related RANS solution Cp for FC7 at various butt-line (BL) positions. As discussed earlier, the flight test data are at a slightly different condition but considered comparable. As is evident in the cross-planes of vorticity away from the air dam or crank, the BL40 through BL95 plots show that the unsteady effects are minimal. BL55, BL70, BL80, and BL95 show good agreement with the available flight test data with only minor discrepancies near the recovery from the strong suction peak. The suction peak Cp value and the position of the peak are in good agreement for all these BL locations. BL105 is located just inboard of the air dam/actuator pod and a small amount of unsteadiness is observed as evidenced by a widening of the minimum Cp, and maximum Cp curves from the mean Cp and RANS Cp curves. At BL127.5, BL153.5, and BL184.5, there are large differences in the minimum Cp and maximum Cp from the mean Cp curves, especially near the vortex-induced suction peak, although the mean Cp curve compares well with the flight-test data. At BL127.5 and BL184.5 we begin to see the difference between the mean Cp computed from a time accurate solution and the RANS Cp. This is especially evident at BL184.5 in the range of x/c from 0.1 to 0.4. In this region, there is a large 'hump' with the time-averaged Cp showing the best agreement with the flight test. This discrepancy has been observed in other fighter aircraft simulations and is typically due to the inability of the RANS turbulence models to accurately capture the effect of the massive separation and strong unsteady vortices [**12**, **14**, **15**, **44**, **45**].

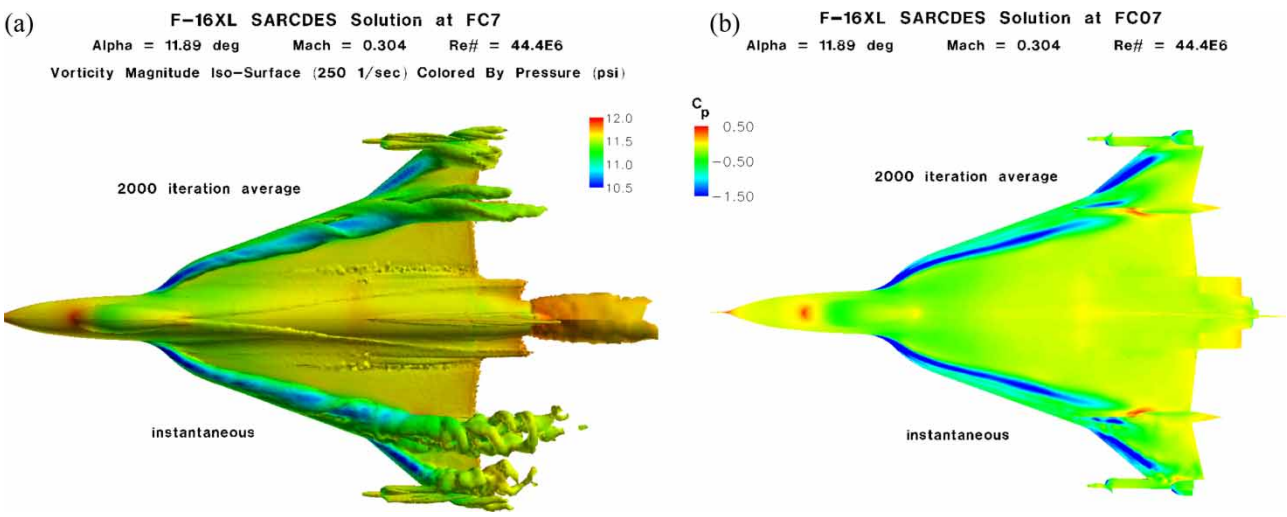

Fig. 6 Comparison of an instantaneous solution to a solution time averaged after 2000 time steps: (a) iso-surfaces of vorticity magnitude coloured by pressure and (b) surface pressure coefficient distribution, Cp

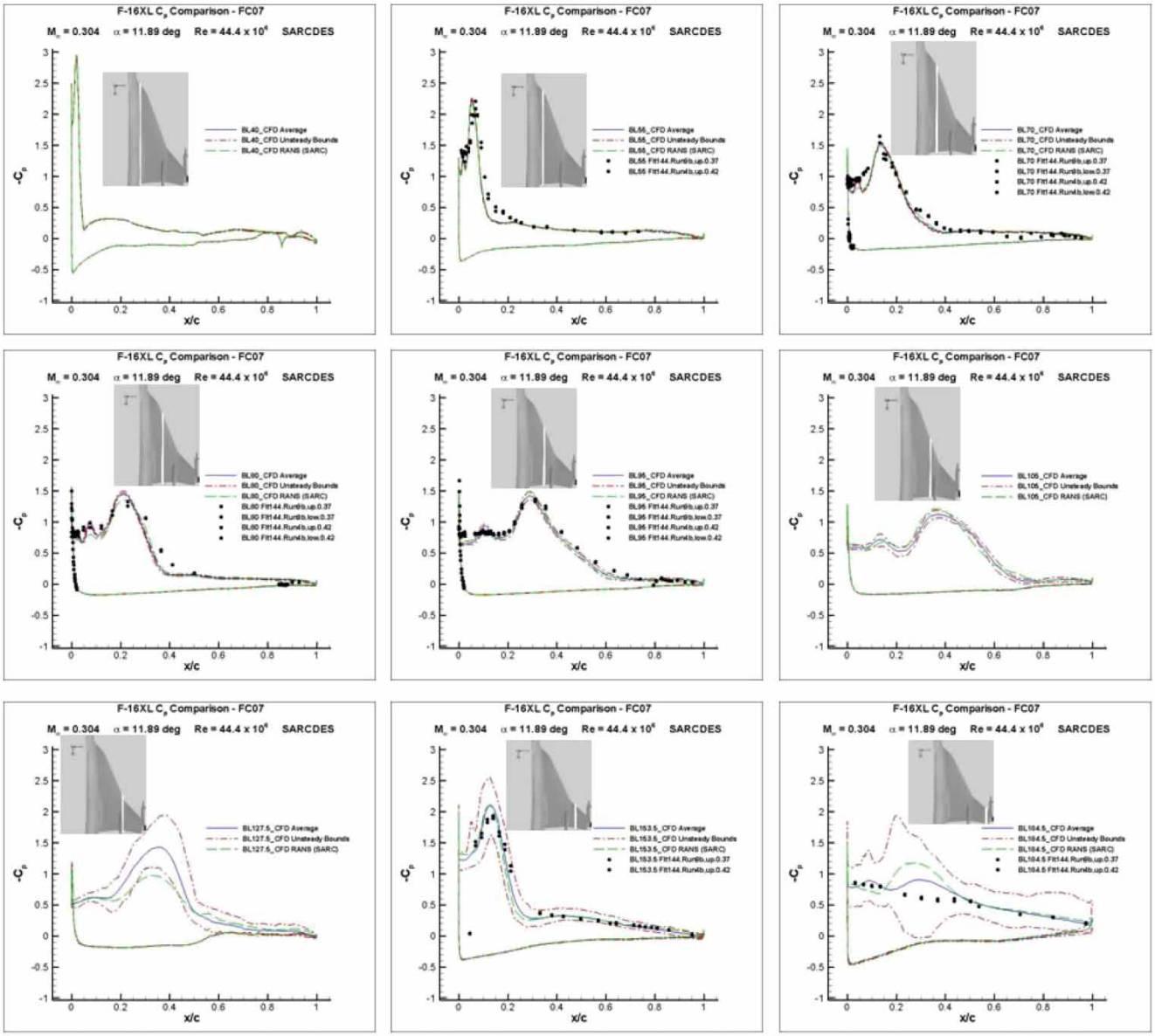

Fig. 7 Flight condition 7; surface *C*p along various F-16XL BL stations for flight test, computed mean, and computed maximum and minimum value for a series of time-accurate solutions

3.4.2 F-18 HARV

The F-18 high angle-of-attack research vehicle (HARV; see Fig. 8) has been proven to be an excellent source of data for researchers working on high angle-of-attack flowfields [**46**, **47**]. Extensive flight testing of the HARV has been conducted that provides a rich source of flow visualization, surface pressures, and aeroelastic information [**48**]. The F/A-18 utilizes wing leading-edge extensions (LEX) to generate vortices that enhance the wing lift, and the twin vertical tails are canted to intercept the strong vortex field and increase manoeuverability. At large incidence, the LEX vortices breakdown upstream of the vertical tails, resulting in a loss of yaw control power and severe aeroelastic effects [**49**]. The ultimate goal of computationally modelling the flowfield, shown in Fig. 8, would be to accurately simulate the aeroelastic impact of the LEX vortices on the twin vertical tails. Previous predictions of the HARV flowfield include RANS computations with solid tails [**50**], DES predictions showing the impact of the breakdown region on the vertical tails [**51**], and fully aeroelastic tails with laminar off-body flow and flow control methods for alleviating tail buffet [**52**]. The current level of the simulation technology, however, has not allowed for accurate prediction of vortex breakdown and the unsteady flow downstream of breakdown at flight Reynolds numbers. Because of this, researchers have spent time computing flows over simpler geometries, such as slender forebodies and delta wings, to improve their simulation capabilities. However, the advent of hybrid turbulence models may finally allow

Fig. 8 NASA F-18 high angle of attack research vehicle . Photo courtesy of NASA-Dryden

for the accurate prediction of full-aircraft flowfields at high incidence.

A detailed numerical investigation of the F-18 HARV flowfield was undertaken to determine the turbulence model requirements for accurate prediction of the flow impinging on the vertical tails [**53**]. All F/A-18C cases were run at 30° angle of attack, a Mach number of 0.28, and a standard day altitude of 20 000 ft. The resulting Reynolds number was 13 million based on the mean aerodynamic chord of the aircraft (12 ft). The leading-edge flaps were set to −33° and the trailing-edge flaps were undeflected in order to match the flight conditions. Turbulence models evaluated included SA, Menter's shear stress transport model (SST), and DES. An adaptive mesh refinement capability was used to ensure that the vortical flow regions had appropriate grid support for the type of aeroelastic flow computations being performed (see reference [**53**] for details about the grid).

The flight test and SADES simulation port pressures were analysed with MATLAB's PSD function. Since the flight test data have a different time step and period of time (40 s), the power resulting from a PSD analysis will not be a one-to-one match, but the frequencies and characteristic shapes of the PSD should match. All 32 flight test pressure port locations were analysed but only Ports 17 and 18 are shown here (see reference [**53**] for more results), which correspond to a position on the vertical tail at 50 per cent span and 90 per cent chord (both inboard and outboard). Figure 9 depicts the comparison of SADES and flight-test data. The frequency content shows quite good comparison between the flight test and SADES simulations. A wide peak amplitude range corresponding to Strouhal numbers between 0.45 and 0.8 is seen for both flight test and SADES simulations. This frequency range corresponds to pressure sweeps over the tail surface observed in a movie clip of the SADES simulation. Unfortunately, the published first bending mode of the vertical tail is at a Strouhal number of ∼0.66, explaining why the tail is so aeroelastically active at this flight condition. The results also show matches in slopes of the PSD for the Strouhal range of 1–10. A consistency is noted in the level of power between inboard and outboard ports for both flight test and SADES, i.e. when the inboard port has a higher power for the flight test that is true as well for the SADES simulation. Finally, when the curves cross, this occurs at approximately the same frequency for the flight test and SADES. The overall comparison of the frequency content is remarkably good for the SADES solutions, demonstrating the utility of the method for tail buffet computations at flight Reynolds numbers [**53**].

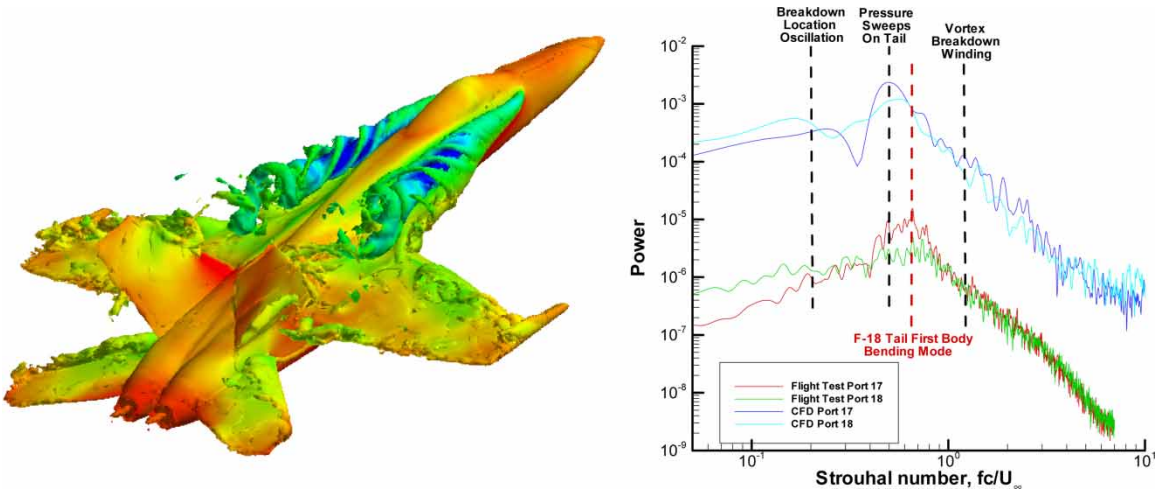

Fig. 9 (a) Isometric views of the F/A-18C at $\alpha = 30°$, DES model, isosurface of vorticity coloured by pressure and (b) comparison of power spectrum density from flight test and DES, Ports 17 and 18 (50 per cent span, 90 per cent chord, and inboard and outboard)

A common definition of vortex breakdown is the location where the streamwise velocity component is zero in the core. The coordinates of this point along the core were tracked in time for each of the methods, SST, SA, and SADES. Figure 10 depicts the time histories of the three methods as well as the flight test and experiment maximum and minimum mean values of vortex breakdown presented in reference [**54**]. Three things are obvious from Fig. 10. First, the amplitude of oscillation for the SST and SA models is almost negligible compared to the SADES simulation. Second, the SST solution predicts the breakdown far upstream of the flight test or experimental values, whereas the SA solution predicts the breakdown location downstream of the flight test and experimental results. Third, the SADES solution gives a mean value of vortex breakdown location well within the flight test and experimental data. It should also be noted that the computed non-dimensional primary frequency of the breakdown oscillation is 0.2, well within the range of frequencies commonly found in the literature for vortex breakdown [**55**]. This inability of commonly used turbulence models to accurately compute a solution with breakdown is well documented in the literature and is due to the large amount of eddy-viscosity that these models put into the core of vortices [**55**]. Several researchers have proposed fixes to these turbulence models by incorporating some form of a rotation correction. The disadvantage of this approach is the fact that the simulation will still be operating in a RANS mode and compute solutions that are relatively steady post-breakdown as opposed to an LES approach that resolves the eddies that produce the unsteadiness. It is clear in Fig. 10 that the SADES method does not suffer from the same problem as the RANS methods due to the fact that eddy viscosity is computed based on sub-grid scale turbulence, automatically minimizing the amount of spurious eddy-viscosity that is placed in the core of vortices.

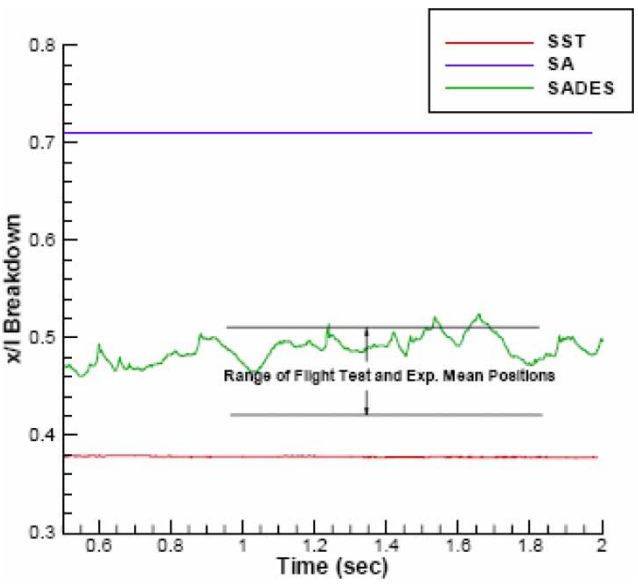

Fig. 10 Time histories of the streamwise coordinate of vortex breakdown referenced to the vehicle's nose and scaled by the length for the SST, SA, and SADES methods

3.4.3 F-16C

While the first two examples demonstrate the accuracy and abilities of high-fidelity CFD techniques, this last example demonstrates the reduced-order, nonlinear loads modelling process discussed previously. The main difference in the CFD computations associated with this example versus the first two examples is that these simulations include a rigid-body grid motion to implement a prescribed aircraft motion. While only stability derivatives are addressed in this example, work is ongoing to implement moving control surfaces in order to investigate control derivatives and associated issues.

To date, a full-scale F-16 undergoing a number of different prescribed motions has been simulated. These 'computational manoeuvres' include continuous α sweeps, sinusoidal pitching, coning motion, oscillatory coning, vertical plunge pulse, vertical plunge chirp, pitch chirp, Schroeder plunge, yaw chirp, composite pitch-yaw chirp, and various notional motions inspired from flight test manoeuvres (e.g. sideslips or pitch doublets). The required motion files for *Cobalt* were defined using an interactive GUI, and the computations were accomplished at Mach numbers ranging from subsonic ($M = 0.3$–0.6) to transonic ($M = 0.85$–0.95) to supersonic ($M = 1.2$) at a Reynolds number (Re) of $\sim$15 million. Many of these manoeuvres have been covered in detail in previous articles [**32**, **56**–**59**] but the current article will discuss only on the α sweeps and a typical pitch chirp manoeuvre with a linear variation in frequency as defined previously. Note that the numerical values on the axes of some of the plots in the following sections have been removed to allow presentation in the open literature.

As in the previous section, all solutions were computed using *Cobalt* V3.0 from Cobalt Solutions limited liability corporation (LLC). Steady-state solutions and initiation of time-accurate solutions were computed using the Reynolds-averaged Navier–Stokes (RANS) turbulence model of SARC, first-order accuracy in time, and a time step commensurate with a Courant–Friedrichs–Lewy (CFL) number of one million. Time-accurate solutions were computed with the DES hybrid RANS-LES turbulence model with SARC as the underlying RANS model. A time-step size of 0.0005 s was chosen as a conservative estimate for all of the time-accurate simulations with the exception of some of the scale-model simulations where a time step of 0.0002 s was used.

All of the computations were run on 128–256 CPUs on three different supercomputing systems. All of the static solutions were accomplished on 'jvn' at the US Army Research Lab in Aberdeen Proving Ground, Maryland. This machine is a Linux Networx Evolocity II with 2048 Intel Xeon EM64T processors running at 3.6 GHz and connected via Myrinet. The dynamic solutions were accomplished either on 'falcon', a 2048-processor AMD Opteron (2.8 GHz) cluster with 1024 XC compute nodes (two processors/node) connected with Infiniband interconnect or 'jaws' at a 5120-processor Dell PowerEdge 1955 blade server cluster (3.0 GHz, dual core) with Infiniband interconnect. Falcon is located at the Aeronautical Systems Center in Dayton, Ohio, and jaws is located at the Maui High Performance Computing Center in Hawaii.

3.4.3.1 α-sweeps. As discussed in reference [**59**], a number of angle of attack sweeps up to 60° were accomplished at various pitch rates. Figure 11 shows the normal force coefficient as a function of angle of attack for 30 and 60°/s pitch rate computations on the full-scale grid and 60 and 120°/s pitch rate computations on a 1/9th-scale grid. From these data, it would be very easy to determine the C_{L_α} derivative in the linear range. Looking at the results for the different α-sweeps, one could also determine the C_{L_q} derivative by noting the linear variation with change in pitch rate (seen more clearly in reference [**59**]). Note that beyond 12.5° angle of attack, the flow regime is unsteady and non-linear, distorting the meaning of these two derivatives. The unsteadiness is inherent to the flow and is not caused by the grid motion but rather by massive separation, vortex breakdown, and vortex interactions. Here, we model this non-linear/unsteady behaviour using other, more complex dynamic motions and non-linear SID techniques (demonstrated later).

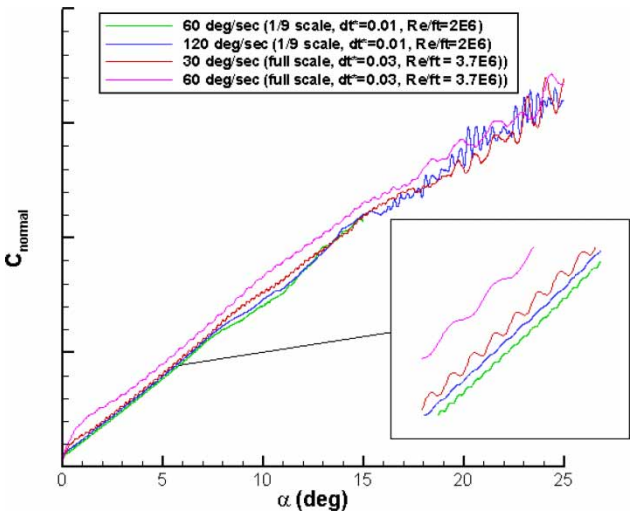

Fig. 11 F16C normal force coefficient data for α sweeps at different pitch rates

Another interesting thing to note in Fig. 11 is the differences in the normal force curves for the full-scale F16C relative to the 1/9th-scale grid. It is clear that the full-scale computations result in a larger amount of pitch-induced lift, and it appears that the required pitch rate must scale along with the grid size when performing sub-scale motion calculations. This has far reaching implications with regard to properly determining the dynamic behaviour of the full-scale aircraft using a sub-scale model (e.g. in a wind tunnel). As a crude example based on Fig. 11, to model a 30 °/s pitch rate on the full-scale aircraft using a 1/9th-scale model, a pitch rate of ∼250°/s would be required. This sort of pitch rate is not realistically obtainable in nominal test facilities. It is important to note that this result is qualitative in nature and no time-step or validation studies have been accomplished with regard to these α-sweep manoeuvres. Still, it is clear that equivalences must be made between non-dimensional versions of rotation rates when accomplishing aerodynamic comparisons between dynamic tests and prescribed motion simulations.

3.4.3.2 Pitch chirp manoeuvre and SID model generation. Figure 12 shows four instantaneous snapshots taken during a linear pitch chirp manoeuvre as defined by equation (1) and similar to the motion depicted in the left-hand pane of Fig. 4. The chirp input signal was used to drive the pitch motion of the grid for the dynamic solution. The chirp signal was defined at a time step of 0.0005 s (identical to solver time step) for 5 s, and linearly spanned the frequency band from 0 to 5 Hz. A total of 10 000 time-accurate time steps were required to accomplish the entire pitch chirp manoeuvre. Five sub-iterations were accomplished at each time step for this manoeuvre. Using 128 processors on 'falcon', a single iteration took ∼6 s of wall time.

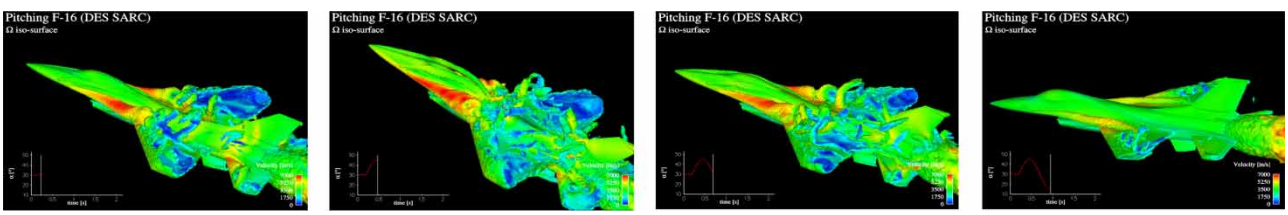

Fig. 12 DES of F-16 in sinusoidal pitching motion of the initial stages of a pitch chirp manoeuvre; instantaneous vorticity iso-surface coloured by magnitude of velocity

The flowfield is seen to be unsteady even at the beginning of the simulation where the angle of attack is static. This is due to the strake vortex experiencing vortex breakdown, and the massive flow separation over the main wing. At dynamic angles of attack, the flowfield undergoes drastic changes, including the appearance and disappearance of a forebody vortex, the burst and reformation of the strake vortex, and the formation of a burst main-wing vortex. These non-linear phenomena give rise to non-linear behaviour of the aerodynamic forces and moments.

Figure 13 shows the normal force coefficient time history resulting from such a chirp manoeuvre (blue line). These data are referred to as the 'training data' in that the input grid motion data, expressed in terms of angle of attack, α, pitch rate, q, and angular acceleration, $\dot{q}$, are used together with the normal force coefficient output data to compute an analytic aerodynamic model using the SID tools described previously. The output data from the CFD solution of the DC chirp were processed using the SIDPAC software allowing terms up to fourth order. The resulting non-linear equation structure for CL as a function of α, q, and $\dot{q}$ is expressed in equation (2) and required 15 terms to fit. The terms in equation (2) are ordered by importance to the model (i.e. the constant term is the most important, α coefficient is the next important, etc.)

$$\begin{aligned} C_{\mathrm{L}}(\alpha, q, \dot{q}) = {} & C_1 + C_2\alpha + C_3 q + C_4\dot{q} + C_5\alpha q^2 \\ & + C_6\alpha q + C_7\alpha\dot{q} + C_8\alpha^3 + C_9 q\dot{q} + C_{10}q^3 \\ & + C_{11}\alpha q\dot{q} + C_{12}\dot{q}^2 + C_{13}q^2\dot{q} + C_{14}\alpha\dot{q}^2 \\ & + C_{15}q^4 \end{aligned} \tag{2}$$

The red line in Fig. 13 shows the model fit of equation (2). It is clear that the model is able to represent the dynamics in the normal force coefficient very well, even at highly transient peak areas where a simple least-square model fit fails, as seen in Fig. 13. An analytic model for pitch moment coefficient (C_{M}) was also identified using SIDPAC, and the resulting equation (equation (3)) required 23 terms

$$\begin{aligned} C_{\mathrm{M}}(\alpha, q, \dot{q}) = {} & C_1 q + C_2 + C_3\alpha^2 + C_4 q^4 + C_5\dot{q} \\ & + C_6\alpha q\dot{q} + C_7\alpha\dot{q}^2 + C_8\alpha + C_9 q^2 + C_{10}\alpha^4 \\ & + C_{11}\alpha^2 q^2 + C_{12}\alpha q^2 + C_{13}q^3\dot{q} + C_{14}q\dot{q}^2 \\ & + C_{15}\alpha^3 q + C_{16}\alpha q\dot{q}^2 + C_{17}\dot{q}^3 + C_{18}\dot{q}^2 \\ & + C_{19}\alpha q + C_{20}\alpha q^3 + C_{21}\alpha\dot{q} + C_{22}\alpha\dot{q}^3 \\ & + C_{23}q\dot{q} \end{aligned} \tag{3}$$

Looking at equations (2) and (3), it is clear that the polynomial models contain non-linear terms and are therefore capable of modelling complex aerodynamic phenomena as long as it is time invariant in nature. Also, while these models could be used to efficiently predict force and moment coefficients as a function of the given input parameters, they could also be directly differentiated to produce analytic models for any desired stability derivative as a function of the model parameters. This will provide much smoother derivative calculations versus numerically differentiating the output data.

3.4.3.3 Model prediction. For validation purposes, single-point solutions were computed for a range of angles of attack from 0 to 30° at a Mach number of 0.6 and an altitude of 5000 ft. An initial steady-state solution was accomplished followed by 3000 time-accurate iterations with second-order temporal and spatial accuracy and three Newton sub-iterations per time step. From this converged solution, an additional 4000 time steps were computed at each angle of attack up to 15°. The converged solution at 15° was used to initialize the remainder of the static runs. Each time-accurate iteration took ~5.7 s using 128 processors on 'jvn'. Typically, the last 2000 iterations of each run were time averaged to compute the aerodynamic coefficient values reported in the results. The unsteady bounds shown in the results were taken as the minimum and maximum values observed over the same number of iterations.

Additionally, to provide static and dynamic experimental validation data, Lockheed Martin's Aircraft Trim, Linearization and Simulation (ATLAS) program was used to compute force and coefficient data at the same parameter values. The ATLAS program is a generalized, 6 DOF, non-linear, and non-real-time simulation. Using ATLAS, the S&C engineer is able to trim the aircraft at a selected flight condition, calculate linear aerodynamic derivatives, and simulate time history response from a trimmed condition for a variety of

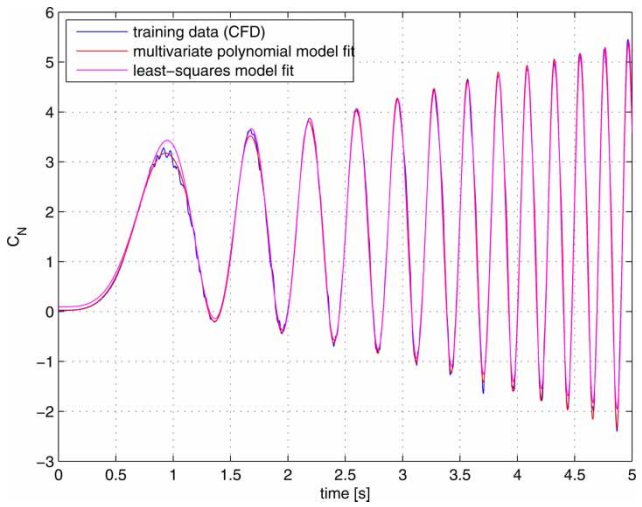

Fig. 13 SID of DC chirp in pitch: training data (from CFD) and model fit. Independent variables are angle of attack, α, pitch rate, q, and angular acceleration, $\dot{q}$

manoeuvres. In addition to performing the aforementioned trims and manoeuvre simulations, force and moment coefficient data can be extracted for further analysis.

It is important to realize that these comparisons are cursory in nature and represent an initial attempt at verification and validation since there is no grid sensitivity study and the configuration is slightly different from the ATLAS configuration. The ATLAS configuration includes wing tip and underwing pylons, whereas the CFD model is a clean configuration. Also, the propulsion system is only an approximation obtained from the open literature, whereas the ATLAS propulsion system is a Lockheed Martin proprietary model.

Figure 14 shows the variation in C_L and C_M as a function of α, as well as C_D as a function of C_L for CFD time-averaged solutions, CFD unsteady maximum and minimum values, ATLAS, and predictions from models generated from the chirp motion simulation. The left-hand side of Fig. 14 depicts the C_L and C_M versus α. C_L and C_M values resulting from solutions up to an α of 15° compare very well with ATLAS and exhibit essentially no unsteady effects as measured by the difference between the minimum, maximum, and average CFD solutions. C_L and C_M values resulting from solutions above an α of 15° exhibit significant unsteadiness and the C_L resulting from time-averaged CFD has a measurable difference from the ATLAS solutions >20° α. This difference may be due to either an insufficient refinement of the grid to capture some relevant physics or the difference in configuration between the CFD grid and ATLAS. As one might expect, the model predictions fall very close to the time-averaged CFD values, demonstrating the ability of these chirp-generated models to predict the static data. The drag coefficient, C_D, as a function of C_L is presented in the right-hand side of Fig. 14. The CFD solutions and model predications compare very well for low values of CL but overpredict the drag for the mid-range of CL and underpredict the drag for the solutions computed at the highest α's. In general, the comparisons are reasonable and demonstrate the usefulness of the CFD-based models for predicting static force and moment coefficient values.

With regard to dynamic validation of the analytical models, Fig. 15 shows the normal force coefficient as a function of the angle of attack computed for constant frequency sinusoidal pitch oscillation at 2 Hz. For this case, the dynamic lift curve (blue) features a wide 'hysteresis' loop that occurs because the flow at increasing angle of attack features different characteristics different from that at decreasing angle of attack. The 'jump' in the lift coefficient at the beginning of

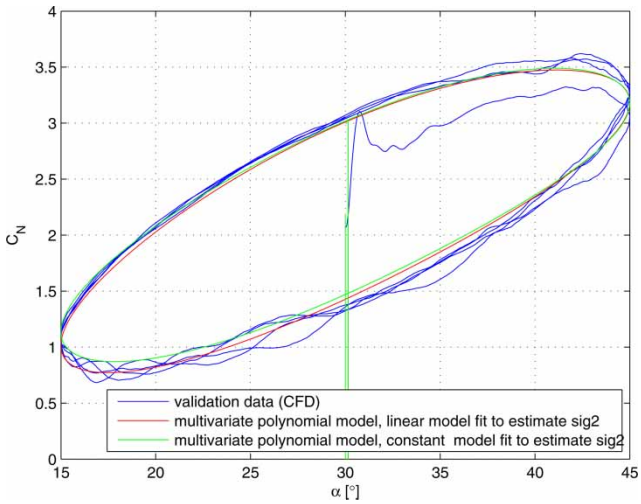

Fig. 15 Validation of pitch chirp in pitch-trained models for normal force coefficient with sinusoidal pitch data, $f = 2.0$ Hz

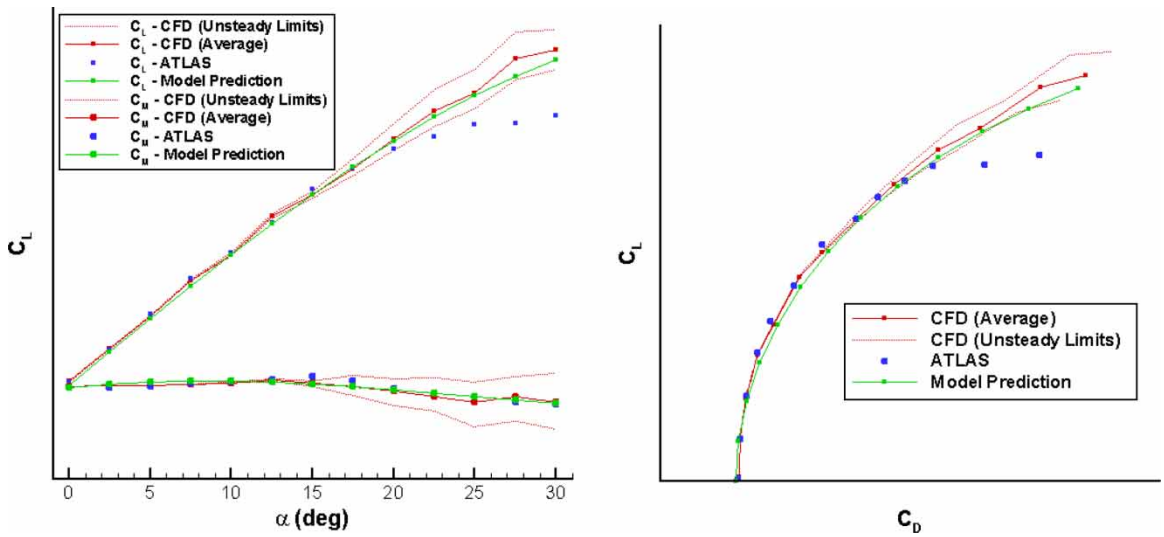

Fig. 14 Lift, drag, and moment coefficients for CFD simulations and CFD models compared to ATLAS

the first cycle is due to the infinite acceleration that occurs when the sinusoidal motion starts. The infinite acceleration is due to a discontinuity in the second derivative of the angle of attack. As a result, the lift coefficient increases from its static value to the dynamic value that corresponds to the angle of attack rate given by the sine wave. The associated transient is seen to have disappeared in the second cycle. Also shown in Fig. 15 is the prediction of two similar variants of the non-linear model identified earlier. The model predictions compare very favourably with the validation data throughout the entire pitch cycle, and the width of the hysteresis loop is matched.

Figure 16 depicts C_L and C_M as a function of time for the pitch chirp manoeuvre. The ATLAS values are only shown for the range of validity of the model resulting in the data drop out at the peaks and valleys of C_L and in between the peaks of C_M. In general, there is a qualitative match between the unsteady CFD, SIDPAC non-linear model of the CFD, and ATLAS. In the C_L versus time plot presented in the left-hand side of Fig. 16, one can see the match in frequency between the three datasets but ATLAS solutions exhibit an additional behaviour between the peaks and valleys not observed by either the CFD or SIDPAC solutions. The C_M versus time results in the right-hand side of Fig. 16 again show a good match in the frequency, but the valleys show an underprediction in the negative C_M values corresponding to the static solution discrepancies in C_M at values corresponding to the static solution α's $> 15^\circ$ as observed in Fig. 14.

After obtaining the SIDPAC model of the F-16, solutions were computed with the model for sinusoidal pitching about a $15^\circ\,\alpha$ with frequencies of 1, 2, and 3 Hz and compared to ATLAS (analogous to Fig. 15). Figure 17 depicts C_L and C_M for the 1 Hz pitching manoeuvre. The C_L as a function of α is presented in the left-hand side of Fig. 17. The simulation starts at an α of 15°, follows the lower portion of the right-hand C_L loop to the right during the up stroke, follows the upper portion of the right-hand loop during the down stroke until $15^\circ\,\alpha$ at which point it crosses to the lower portion of the left-hand loop until a $0^\circ\,\alpha$. The up stroke from $0^\circ\,\alpha$ follows the upper portion of the left-hand curve until reaching $15^\circ\,\alpha$ again. As one can see, the orientation of the two loops are matched with the ATLAS simulation showing a collapsed loop on the lower angles of attack and a loop with a lower C_L on the upper end of α values. These differences correspond to the differences seen in the time history of C_L presented in Fig. 16. On the other hand, the C_M values are in quite good agreement with a match in the orientation of the loops and even a match in values as well. This is surprising since the C_M time history from CFD shows measurable differences relative to ATLAS.

3.4.3.4 Mutli-axis manoeuvre inputs. The above example has demonstrated the ability to identify an analytic model from a prescribed single-axis simulation motion (pitch chirp). Although it is a fairly simple task to generate prescribed chirp motions about a single axis, it is more desirable to implement such motions in multiple axes so that the resulting models may be used to predict a more complex motion (e.g. yaw-roll manoeuvres). It is ultimately desired to be able to excite the aircraft aerodynamics based on motion in all the three coordinate axes with a single CFD run. The resulting data could then be used to generate a reduced-order model for all six force and moment coefficients. Then, these models could be quickly differentiated to provide the needed stability derivatives as discussed previously. Initial research down this path has taken place during recent months.

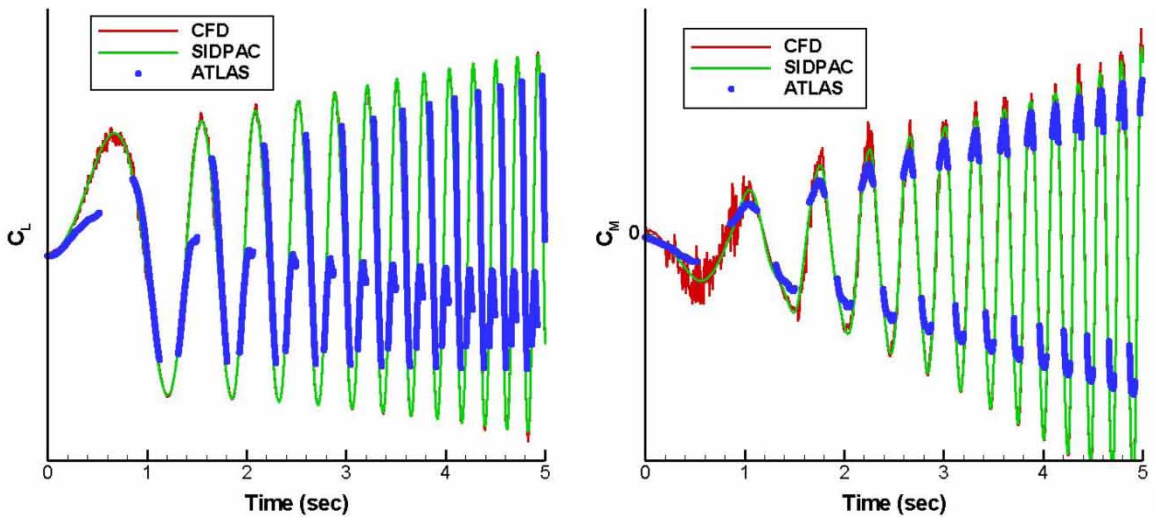

Fig. 16 Lift and moment coefficient as a function of time for CFD, SIDPAC non-linear model of CFD data, and ATLAS

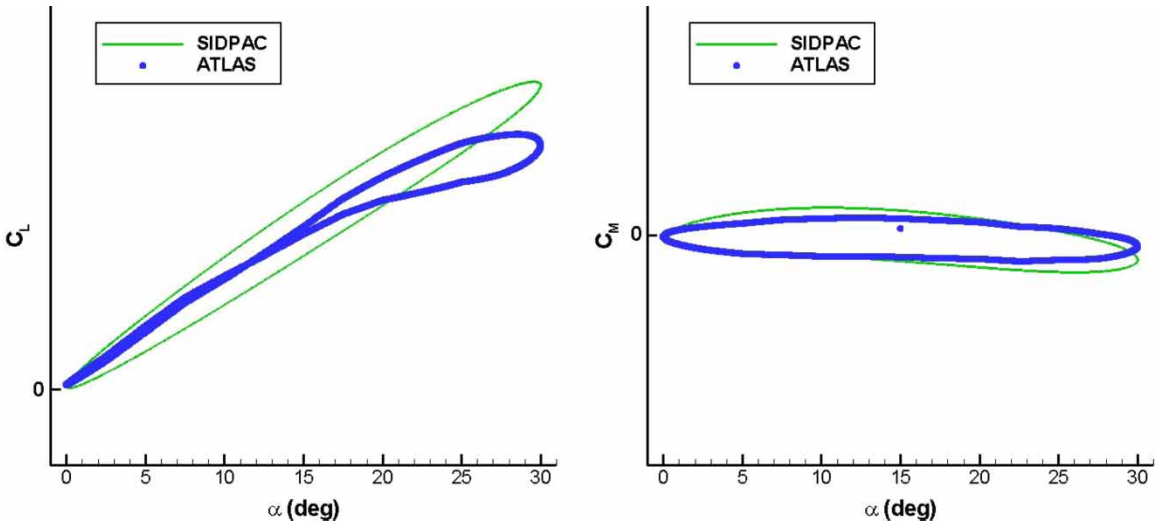

Fig. 17 Lift and moment coefficient data resulting from a sinusoidal pitching manoeuvre symmetric ∼15° at 1 Hz. SIDPAC non-linear model of CFD data trained by a DC chirp manoeuvre compared to ATLAS

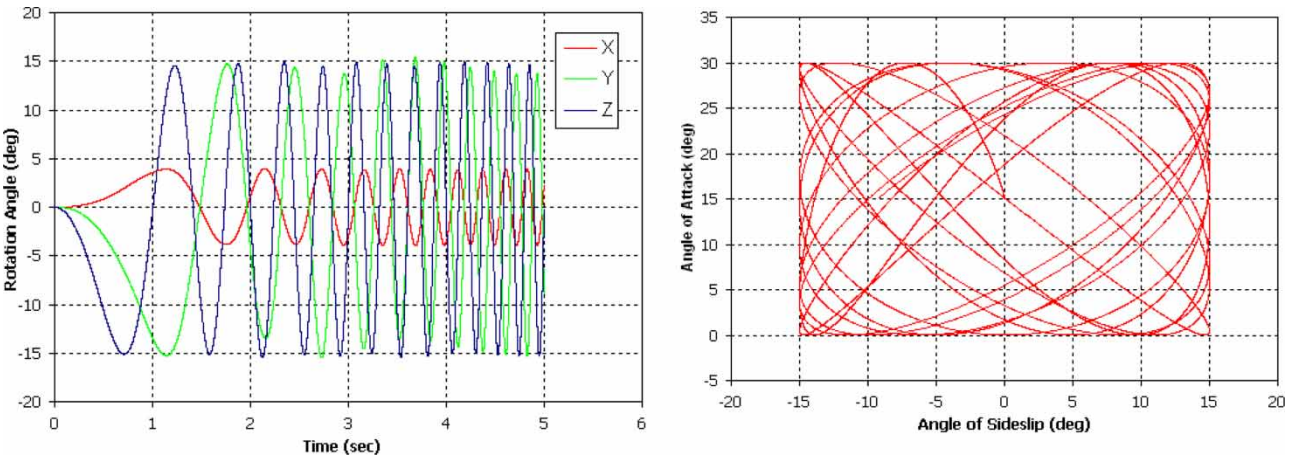

Fig. 18 Grid motion (left) and resulting angle of attack/sideslip (right) for combined yaw-pitch chirp manoeuvre

Figure 18 shows an example of a combined pitch-yaw chirp motion designed to provide angle of attack motion between 0 and 30° and sideslip motion between −15 and +15°. The pitch chirp motion was generated with $\lambda = 1.0$, and the yaw chirp motion was generated with $\lambda = 1.47$ (computed to make the chirp signals orthogonal). The left pane of Fig. 18 shows the required grid rotations about the three coordinate axes, and the right pane shows the resulting angle of attack and sideslip excursions based on the prescribed flow conditions (0.6 Mach, 5000 ft). Note that motion in all the three coordinate directions is needed since the prescribed yaw motion in this case was about the vertical stability axis versus the vertical body axis. It is clear that this prescribed motion will force the aircraft through a large number of angle of attack/sideslip combinations (and likewise pitch, roll, and yaw-rate combinations). This is a much more efficient way to 'map' the flight envelope with aerodynamic force and moment coefficients versus running multiple static solutions or even single axis motions.

4 CONCLUSIONS

The accurate and efficient determination of the stability and control characteristics of fighter aircrafts is an important element in both the design of new configurations as well as store compatibility clearances of fielded aircrafts. For new aircraft designs, the failure to accurately predict these static and dynamic parameters often leads to a reduction in the number of purchased aircrafts due to cost overruns resulting from problems found late in the design process. For new weapons' clearances, inadequate predictions lead to unwarranted flight envelope restrictions or, in the worst case scenarios, operational mishaps. The use of high-fidelity CFD to complement proven wind-tunnel

and flight test techniques for determining the stability and control characteristics of fighter aircraft has been discussed. Since a bottom-up approach to filling the necessary elements of a stability and control database is not feasible for turbulent Navier–Stokes CFD solutions on full aircraft configurations, it is possible to generate lower-fidelity analytic models capable of modelling the troublesome aerodynamic phenomena that lead to static and dynamic instabilities. Then, these efficient models could be used to perform the desired analyses. Previous results from two different full-aircraft computational and flight-test comparison studies were reviewed, demonstrating that state-of-the-art flow solvers are capable of capturing the non-linear aerodynamic phenomena that lead to stability problems. A relatively new approach by the authors, which couples high-fidelity CFD techniques with proven SID methods, was also demonstrated via F-16C computations and comparisons to the available data. The comparisons were favourable but differences were apparent in some cases, most likely due to known differences between vehicle configurations.

ACKNOWLEDGEMENTS

This work was sponsored by the DoD HPC/AF SEEK EAGLE Office Institute for High Performance Computing Applications of Air Armament . The computational resources were generously provided by various Major Shared Resource Centers within the DoD HPCMP, the Maui High Performance Computing Center , and the Arctic Region Supercomputing Center . The authors gratefully acknowledge Dr Eugene A. Morelli from NASA Langley, who provided the SIDPAC.

REFERENCES

1 **Yurkovich, R.** and **Chen, P. C.** State-of-the-art of unsteady aerodynamics for high performance aircraft. AIAA paper 2001-0428, 2001.

2 **Meyn, L. A.** and **James, K. D.** Full scale wind tunnel studies of F/A-18 tail buffet. *J. Aircr.*, 1996, **33**(3), 589–595.

3 **Jacobson, S. B., Britt, R. T., Freim, D. R.,** and **Kelly, P. D.** Residual pitch oscillation (RPO) flight test analysis on the B-2 Bomber. AIAA paper 1998-1805, 1998.

4 **Mason, W. H.** Stability and control in computational simulations for conceptual and preliminary design: the past, today, and future. In Proceedings of the Computational Methods for Stability and Control Symposium, Hampton, Virginia, 23–25 September 2003.

5 **Dean, J. P., Morton, S. A., McDaniel, D. R.,** and **Görtz, S.** Efficient high resolution modeling of fighter aircraft with stores for stability and control clearance. US Air Force T&E Days, Destin, FL, 13–15 February 2007.

6 **Ward, D. T.** *Introduction to flight test engineering*, 1993 (Elsevier Science B.V., Amsterdam, The Netherlands).

7 **Kimberlin, R. D.** *Flight testing of fixed-wing aircraft*, 2003 (AIAA Educational Series, Reston, Virginia, USA).

8 **Stinton, D.** *Flying qualities and flight testing the airplane*, 1996 (AIAA Educational Series, Reston, Virginia, USA).

9 AGARD Advisory Report 305. Fluid dynamics panel working group 16. Cooperative programme on dynamic wind tunnel experiments for maneuvering aircraft, 1996.

10 **Pamadi, B. N.** *Performance, stability, dynamics, and control of airplanes*, 1998 (AIAA Educational Series, Reston, Virginia, USA).

11 **Stevens, B. L.** and **Lewis, F. L.** *Aircraft control and simulation*, 2nd edition, 2003 (John Wiley & Sons Inc., Hoboken, New Jersey, USA).

12 **Forsythe, J. R., Hoffmann, K. A., Cummings, R. M.,** and **Squires, K. D.** Detached-eddy simulation with compressibility corrections applied to a supersonic axisymmetric base. *J. Fluids Eng.*, 2002, **124**(4), 911–923.

13 **Forsythe, J. R.** and **Woodson, S. H.** Unsteady computations of abrupt wing stall using detached-eddy simulation. *J. Aircr.*, 2005, **42**(3), 606–616.

14 **Morton, S. A., Forsythe, J. R., Mitchell, A. M.,** and **Hajek, D.** Detached-eddy simulations and Reynolds-averaged Navier–Stokes simulations of delta wing vortical flowfields. *J. Fluids Eng.*, 2002, **124**(4), 924–932.

15 **Forsythe, J. R., Squires, K. D., Wurtzler, K. E.,** and **Spalart, P. R.** Detached-Eddy simulation of fighter aircraft at high alpha. *J. Aircr.*, 2004, **41**(2), 193–200.

16 **Forsythe, J.** and **Woodson, S.** Unsteady computations of abrupt wing stall using detached-eddy simulation. *AIAA J. Aircr.* 2005, **42**(3), 606–616.

17 **Claus, M., Morton, S. A.,** and **Cummings, R.** DES turbulence modelling on the c-130 comparison between computational and experimental results. AIAA paper 2005-884, 2005.

18 **Morton, S. A., Forsythe, J. R., Squires, K. D.,** and **Cummings, R. M.** Detached-eddy simulations of full aircraft experiencing massively separated flows. *Comput. Fluid Dyn. J.* (*ISCFD Japan*), 2005, **13**(3), 2005.

19 **Strang, W. Z., Tomaro, R. F.,** and **Grismer, M. J.** The defining methods of cobalt$_{60}$: a parallel, implicit, unstructured Euler/Navier–Stokes flow solver. AIAA paper 1999-0786, 1999.

20 **Murman, S. M., Chaderjian, N. M.,** and **Pandya, S. A.** Generation of aerodynamic data using design of experiment and data fusion approach. AIAA paper 2002-0259, 2002.

21 **Rogers, S. E., Aftomis, M. J., Pandya, S. A., Chaderjian, N. M., Tejnil, E. T.,** and **Ahmad, J. U.** Automated CFD parameter studies on distributed parallel computers. AIAA paper 2003-4229, 2003.

22 **Tang, C. Y., Gee, K.,** and **Hawke, V. M.** Development of intelligent agents for the generation of aerodynamic data. AIAA paper 2003-0458, 2003.

23 **Tang, C. Y., Gee, K.,** and **Lawrence, S. L.** Generation of aerodynamic data using design of experiment and data fusion approach. AIAA paper 2005-1137, 2005.

24 **Murman, S., Aftosmis, M.,** and **Nemec, M.** Automated parameter studies using a Cartesian method. AIAA paper 2004-5076, 2004.

25 **Murman, S. M.** A reduced-frequency approach for calculating dynamic derivatives. AIAA paper 2005-0840, 2005.

26 **Denegri, C.** FSI requirements and applications. In Proceedings of the CFD/CSM Workshop on Fluid–Structure

Interaction, Eglin AFB/University of Florida REEF Center, 11 April 2007.

27 **Saephan, S.** and **van Dam, C. P.** Determination of dynamic stability information through simulation of a tumbling tailless aircraft. AIAA paper 2006-6131, 2006.

28 **Tomaro, R. F., Strang, W. Z.,** and **Sankar, L. N.** An implicit algorithm for solving time dependent flows on unstructured grids. AIAA paper 1997-0333, 1997.

29 **Grismer, M. J., Strang, W. Z., Tomaro, R. F.,** and **Witzemman, F. C.** Cobalt: a parallel, implicit, unstructured Euler/Navier–Stokes Solver. *Adv. Eng. Softw.*, 1998, **29**(3–6), 365–373.

30 **Karypis, G., Schloegel, K.,** and **Kumar, V.** Parmetis: parallel graph partitioning and sparse matrix ordering library, version 3.1. Technical report, Department of Computer Science, University of Minnesota, 2003.

31 **Spalart, P. R., Deck, S., Shur, M. L., Squires, K. D., Strelets, M. Kh.,** and **Travin, A.** A new version of detached-eddy simulation, resistant to ambiguous grid densities. *Theor. Comput. Fluid Dyn.*, 2006, **20**, 181–195.

32 **Görtz, S., McDaniel, D. R.,** and **Morton, S. A.** Towards an efficient aircraft stability and control analysis capability using high-fidelity CFD. In Proceedings of the Aerospace Sciences Meeting, Reno, Nevada, January 2007, AIAA paper 2007-1053.

33 **Ljung, L.** *System identification: theory for the user*, 2nd edition, 1999 (Prentice-Hall, Upper Saddle River, New Jersey, USA).

34 **Morelli, E. A.** and **Klein, V.** Application of system identification to aircraft at NASA Langley Research Center. *J. Aircr.*, 2005, **42**(1), 12–25.

35 **Klein, V.** and **Morelli, E. A.** *Aircraft system identification – theory and practice*, 2006 (AIAA Educational Series, Reston, Virginia, USA).

36 **Jategaonkar, R. V.** Flight vehicle system identification – a time domain methodology. In *Progress in astronautics and aeronautics* (Ed. F. K. Lu), vol. 216, 2006 (AIAA, Reston, Virginia, USA).

37 **Jategaonkar, R. V. Fischenberg, D.,** and **Gruenhagen, W.** Aerodynamic modeling and system identification from flight data – recent applications at DLR. *J. Aircr.*, 2004, 0021-8669 **41**(4), 681–691.

38 **Morelli, E. A.** Global non-linear parametric modeling with application to F-16 aerodynamics. In Proceedings of the American Control Conference, Philadelphia, Pennsylvania, June 1998, ACC paper WP04-2, paper ID i-98010-2.

39 **Morelli, E. A.** System IDentification Programs for AirCraft (SIDPAC). AIAA paper 2002-4704, 2002.

40 **Lamar, J. E., Obara, C. J., Fisher, B. D,** and **Fisher, D. F.** Flight, wind-tunnel, and computational fluid dynamics comparison for cranked arrow wing (F-16XL-1) at subsonic and transonic speeds. NASA TP-2001-210629, 2001.

41 **Lamar, J. E.** and **Obara, C. J.** Review of cranked-arrow wing aerodynamics project: its international aeronautical community role. AIAA paper 2007-0487, 2007.

42 **Hummel, D.** and **Redeker, G.** A new vortex flow experiment for computer code validation. In Proceedings of the RTO AVT Symposium on Advanced Flow Management; Part A – Vortex Flow and High Angle of Attack, Loen, Norway, 7–11 May 2001, paper number 8.

43 **Morton, S. A., McDaniel, D. R.,** and **Cummings, R. M.** F-16XL unsteady simulations for the CAWAPI facet of RTO task group AVT-113. AIAA paper 2007-0493, 2007.

44 **Mitchell, A. M., Morton, S. A., Forsythe, J. R.,** and **Cummings, R. M.** Analysis of delta-wing vortical substructures using detached-eddy simulation. *AIAA J.*, 2006, **44**(5), 964–972.

45 **Forsythe, J. R.** and **Woodson, S. H.** Unsteady computations of abrupt wing stall using detached-eddy simulation. *J. Aircr.*, 2005, **42**(3), 606–616.

46 **Lee, B. H. K.** Vertical tail buffeting of fighter aircraft. *Prog. Aerosp. Sci.*, 2000, **36**(3–4), 193–279.

47 **Fisher, D., Del Frate, J. H.,** and **Zuniga, F. A.** Summary of in-flight flow visualization obtained from the NASA high alpha research vehicle. NASA TM-101734, January 1991.

48 Ames Research Center Dryden Flight Research Facility. High alpha research vehicle phase II flight report. Flight 197–199. HA94-70-660, February 1994.

49 **Murman, S. M., Rizk, Y. M, Cummings, R. M.,** and **Schiff, L. B.** Computational investigation of slot blowing for fuselage forebody flow control. *Aircr. Des.*, 1999, **2**(1), 45–63.

50 **Gee, K., Murman, S. M.,** and **Schiff, L. B.** Computation of F/A-18 tail buffet. *J. Aircr.*, 1996, **33**(6), 1181–1189.

51 **Morton, S. A., Steenman, M. B., Cummings, R. M.,** and **Forsythe, J. R.** DES grid resolution issues for vortical flows on a delta wing and an F-18C. AIAA paper 2003-1103, 2003.

52 **Sheta, E. F.** Alleviation of vertical tail buffeting of F/A-18 aircraft. *J. Aircr.*, 2004, **41**(2), 322–330.

53 **Morton, S. A., Cummings, R. M.,** and **Kholodar, D. B.** High resolution turbulence treatment of F/A-18 tail buffet. AIAA paper 2004-1676, 2004.

54 **Ghaffari, F.** Navier–Stokes, flight, and wind tunnel flow analysis for the F/A-18 aircraft. NASA TP 3478, December 1994.

55 **Gursul, I.** Review of unsteady vortex flows over delta wings. AIAA paper 2003-3942, 2003.

56 **Morton, S., Goertz, S.,** and **McDaniel, D.** Computational aircraft and armament stability and control techniques applied to the F-16. In Proceedings of the ITEA Store Compatibility Symposium, Destin, Florida, April 2006.

57 **Morton, S. A., Dean, J., McDaniel, D. R.,** and **Görtz, S.** Poster paper on computational aircraft and armament stability and control techniques applied to the F-16. In Proceedings of the International Test and Evaluation Association National Symposium, Orlando, Florida, November 2006.

58 **Morton, S. A., Görtz, S.,** and **McDaniel, D. R.** Computational stability and control analysis of the F-16. Maui High Performance Computing Center Application Briefs, 2006.

59 **Dean, J., Morton, S. A., McDaniel, D. R.,** and **Görtz. S.** Efficient high resolution modeling of fighter aircraft with stores for stability and control clearance. In Proceedings of the American Institute of Aeronautics and Astronautics Air Force Test and Evaluation Days Conference, Sandestin, Florida, April 2007, AIAA paper 2007-1652.